Chemical Science

ROYAL SOCIETY OF CHEMISTRY

EDGE ARTICLE

View Article Online
View Journal | View Issue

Cite this: *Chem. Sci.*, 2021, **12**, 4949

All publication charges for this article have been paid for by the Royal Society of Chemistry

Received 1st February 2021
Accepted 23rd February 2021

DOI: 10.1039/d1sc00602a

rsc.li/chemical-science

Aggregation-free and high stability core–shell polymer nanoparticles with high fullerene loading capacity, variable fullerene type, and compatibility towards biological conditions†

Taejun Eom, ‡[a] Viktor Barát, ‡[b] Anzar Khan [a] and Mihaiela C. Stuparu *[b]

Fullerenes have unique structural and electronic properties that make them attractive candidates for diagnostic, therapeutic, and theranostic applications. However, their poor water solubility remains a limiting factor in realizing their full biomedical potential. Here, we present an approach based on a combination of supramolecular and covalent chemistry to access well-defined fullerene-containing polymer nanoparticles with a core–shell structure. In this approach, solvophobic forces and aromatic interactions first come into play to afford a micellar structure with a poly(ethylene glycol) shell and a corannulene-based fullerene-rich core. Covalent stabilization of the supramolecular assembly then affords core-crosslinked polymer nanoparticles. The shell makes these nanoparticles biocompatible and allows them to be dried to a solid and redispersed in water without inducing interparticle aggregation. The core allows a high content of different fullerene types to be encapsulated. Finally, covalent stabilization endows nanostructures with stability against changing environmental conditions.

Introduction

Fullerenes are a family of carbon cages. They are characterized by high electron affinities, reactive exteriors, and inert interiors.[1–4] The first two characteristics enable them to quench reactive oxygen species, which are considered to be mediators of oxidative stress and cause for numerous chronic and acute diseases.[5] The interior space can entrap metal atoms such as gadolinium to assist in magnetic resonance imaging.[6] This approach of confining the active and toxic metal atoms to the carbon cage allows overcoming the stability and toxicity issues associated with the gadolinium chelates typically used for imaging purposes.[7] However, despite great potential, the applications of fullerenes in biomedical sciences remain rather limited due to their poor water solubility. The general approaches to enhance their water solubility include covalent modification of the exterior and supramolecular complexation with a variety of hosts (Fig. 1).[8–17] The former suffers from unknown toxicological profiles of new fullerene derivatives and complex synthesis involving regio- and stereoisomers. Although

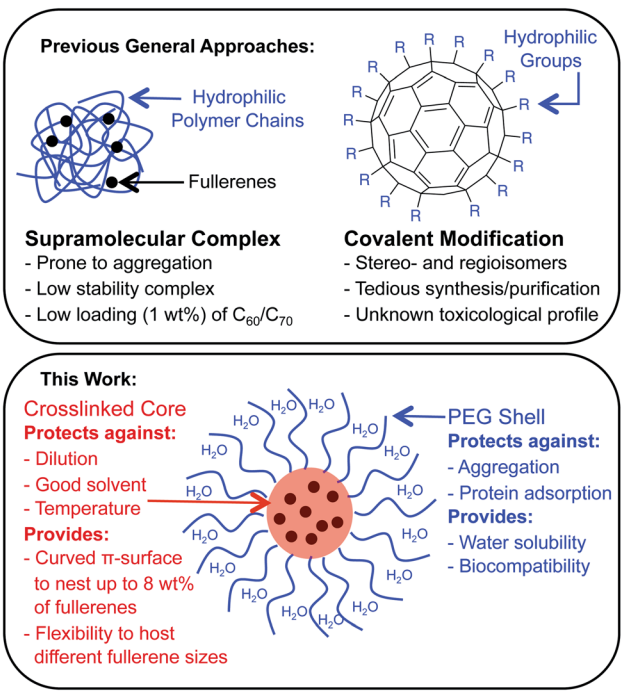

Fig. 1 The most common strategies for preparing water-soluble fullerenes involve supramolecular complexation with a polymer chain or covalent modification of the carbon scaffold (top). The attributes of a fullerene-containing core–shell nanoparticle morphology as explored in this work (bottom).

[a]*Department of Chemical and Biological Engineering, Korea University, 02841 Seoul, Korea*

[b]*Division of Chemistry and Biological Chemistry, School of Physical and Mathematical Sciences, Nanyang Technological University, 21 Nanyang Link, 637371, Singapore. E-mail: mstuparu@ntu.edu.sg*

† Electronic supplementary information (ESI) available. See DOI: 10.1039/d1sc00602a

‡ T. E. and V. B. contributed equally to this work.

great strides have been made recently with the help of 'click' chemistry, which allows for multi-fullerene molecules to be prepared by multi-step organic synthesis.[18] The latter approach suffers from low fullerene loading capacity (~1 wt%) and reduced *in vivo* stability of the noncovalent constructs. Interestingly, C_{70} is shown to be a better candidate in terms of biological applications.[19] However, studies involving C_{70} are scarce due to an even higher restriction on access to water-soluble larger fullerene structures. To address these issues, we designed a covalently stabilized block copolymer micellar system in which (i) host–guest interactions in the micellar core enable a high (8 wt%) fullerene loading capacity (Scheme 1), (ii) the flexibility of the host units and their multiple numbers allow smaller (C_{60}) and larger (C_{70}) guest surfaces to be encapsulated irrespective of their sizes (Fig. 2), (iii) core-crosslinking renders the structures robust against changing environmental conditions, and (iv) a well-defined PEG-based shell provides solvation in water, hemocompatibility, and protection from unfavorable interparticle and protein–particle interactions. A preliminary property study is also carried out, which indicates that C_{70} nanoparticles are more active than C_{60} nanoparticles towards free radical scavenging in aqueous solutions. This observation further reinforces the idea that larger fullerenes offer superior biorelevant properties.

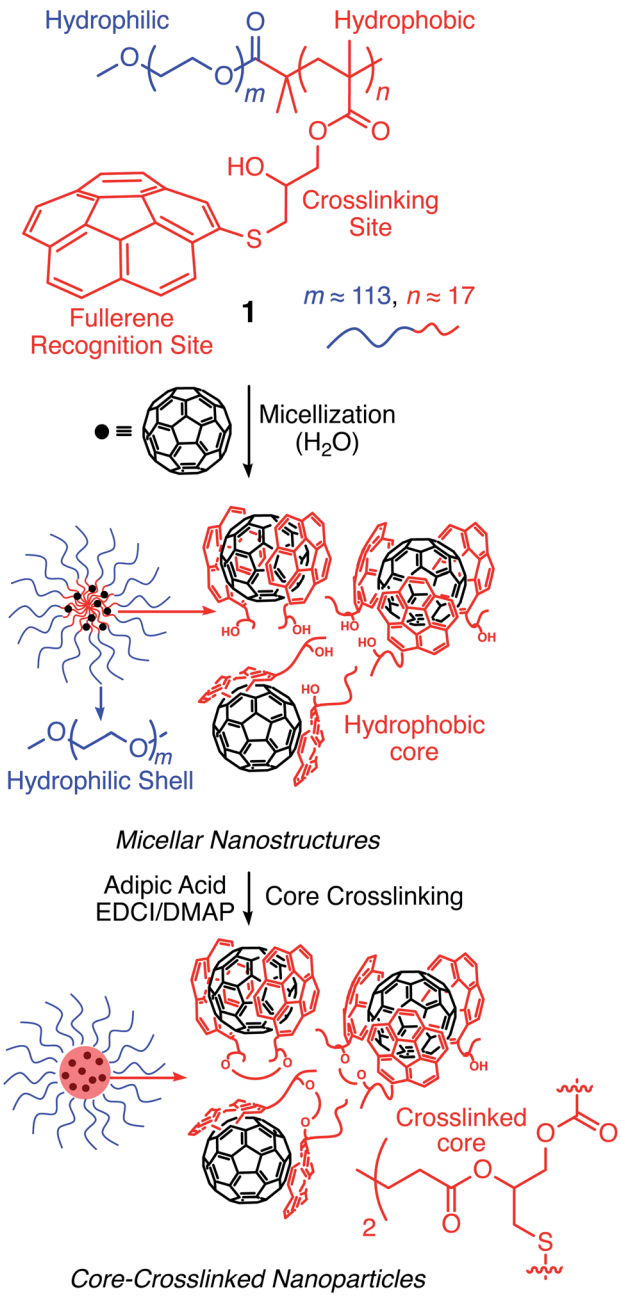

Scheme 1 Chemical structure of host polymer **1** encoded with corannulenes and its assembly with fullerenes through ball-and-socket interactions between concave and convex aromatic surfaces to furnish micellar nanoparticles.

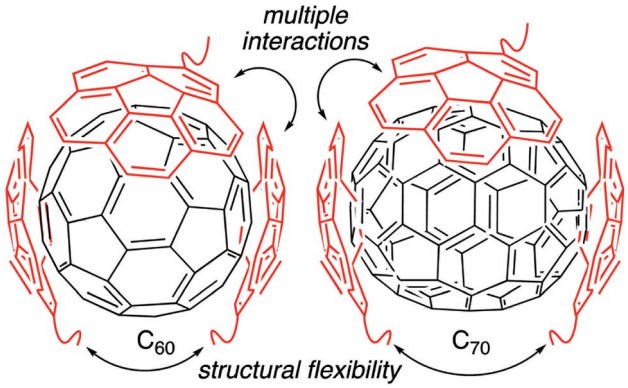

Fig. 2 The hosting polymer block contains many corannulene units attached to the polymer backbone through a linker that can adjust upon receiving the guest molecule. These features allow accommodating different fullerene sizes in the micellar core.

Results and discussion

Molecular design

Corannulene ($C_{20}H_{10}$) can be considered a fragment of fullerene C_{60}.[20] However, its tour-de-force synthesis by Barth and Lawton predates the discovery of fullerenes by nearly two decades.[21] Since then, many properties of this fascinating molecule have been studied, including its capacity to host fullerene C_{60} [22] through complementarity of the curved π-surfaces.[23] To introduce this motif into a polymer chain, a post-polymerization modification strategy was developed (Scheme 2). For this, initially, an atom transfer radical polymerization of glycidyl methacrylate (GMA) monomer through a poly(ethylene glycol) (PEG)-based macroinitiator (PEG-Br) ($M_{n(GPC)} = 8600$, $M_w/M_n = 1.1$) was carried out to access the reactive block copolymer (PEG-*b*-PGMA) scaffold ($M_{n(GPC)} = 12\,700$, $M_w/M_n = 1.2$) (ESI Fig. S1†). Area integration analysis in ^{1}H NMR spectroscopy indicates that the degree of polymerization for the GMA block was approximately 17 repeating units (ESI Fig. S2†). The ring opening reaction between the epoxide group of PGMA and mercaptocorannulene then afforded host polymer **1** ($M_{n(GPC)} = 17\,800$, $M_w/M_n = 1.2$). ^{1}H NMR spectroscopy indicated that the post-synthesis modification reaction was quantitative; therefore,

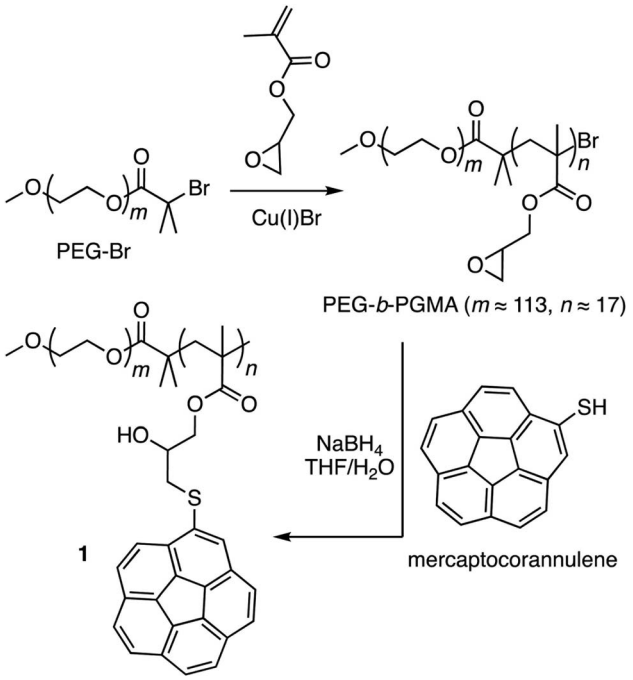

Scheme 2 Synthesis of block copolymer **1** through post-polymerization modification of the reactive poly(ethylene glycol)-*b*-poly(glycidyl methacrylate) scaffold.

approximately 17 corannulene units were incorporated into each diblock copolymer chain. This synthetic strategy was chosen because the ring opening reaction produces a reactive hydroxyl group that could be used for the core-crosslinking reaction once the amphiphilic block copolymer assembles into a micellar nanostructure. The choice of PEG as the shell component was due to its ability to avoid fouling with proteins and to impart water solubility and prolonged blood circulation kinetics to the nanoparticles.[24]

Micelle formation and covalent stabilization[25]

Above a certain concentration, block copolymers carrying hydrophilic and hydrophobic segments can assemble into a micellar structure in a solvent that selectively solubilizes only one of the polymer blocks.[26] The concentration is referred to as the critical micelle concentration (CMC). Micelles can be produced with different morphologies and functions. However, their supramolecular nature makes them susceptible to changing environmental conditions. For example, a solvent that can solubilize both polymer blocks can dissolve the supramolecular structure. In the context of biological applications, shear forces under flow conditions are also expected to disrupt such noncovalent assemblies. Crosslinking of the core or shell is required to stabilize the assembled structure against any changes in solvent, concentration, or temperature. This path leads to robust nanoparticles.[25,27–31]

To study micelle formation from polymer **1** under aqueous conditions, the fluorescence emission of corannulene was monitored at 465 nm. As the polymer chains begin to assemble, the emission signal intensity decreases due to the aggregation-induced self-quenching process.[32] These data allows the determination of the CMC and indicate that at concentrations above 12 μg mL^{-1}, polymer **1** forms micellar structures (Fig. 3). Dynamic light scattering (DLS) studies were undertaken to investigate the micellar sizes. In dimethylformamide (DMF), a good solvent for both polymer blocks, a hydrodynamic diameter of <1 nm indicated individual polymer chains in the solution. In water, a solvent preferential for the poly(ethylene glycol) block, larger structures with an average hydrodynamic diameter of 37–38 nm could be observed, indicating micellar assembly. These micelles could be stabilized through crosslinking of the hydroxyl groups present in the core with adipic acid using 1-ethyl-3-(3-dimethylaminopropyl)carbodiimide (EDCI) as the carboxyl activating agent and dimethylaminopyridine (DMAP) as the catalyst for the formation of the ester bonds. Upon crosslinking of the core, the micellar size decreased slightly (31–32 nm). This is most likely due to crosslinking-induced shrinkage of the core.

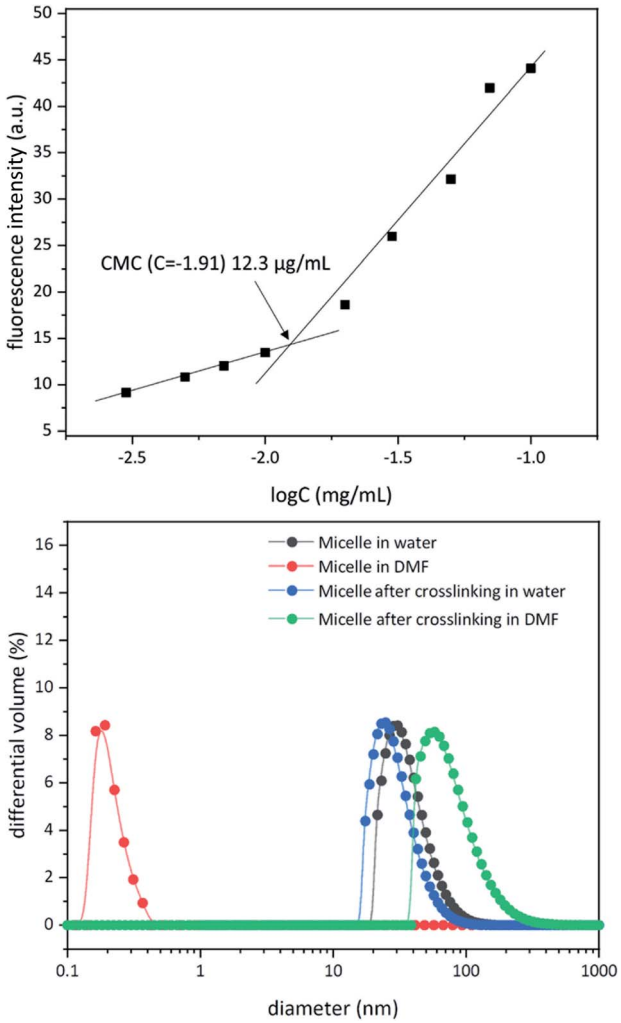

Fig. 3 Critical micelle concentration for polymer **1** (top). Dynamic light scattering data for micellization before and after core crosslinking process in water and dimethyformamide (bottom).

Since, such an intermolecular crosslinking process requires a very low fraction of the reactive sites, and the polymer chains

contained the ester groups already (before formation of new ester bonds upon core-crosslinking), typical characterization tools such as NMR and IR spectroscopies were found to be of no help in characterizing the crosslinked structure. However, the success of the crosslinking process could be verified by dissolution of the micelles in DMF – a solvent that is good for both polymer blocks and therefore capable of solubilizing the supramolecular micellar assembly into individual polymer chains (Fig. 3). Upon crosslinking, the micelles could be dispersed in DMF without destroying the nanostructure (Fig. 3). This indicated that the crosslinking process was successful in covalently stabilizing the micellar structure. However, larger particle sizes were observed (82–83 nm), presumably due to swelling of the crosslinked core in DMF.

Fullerene loading

Two different approaches were examined to incorporate fullerenes into the micellar structures (Fig. 4). In the first approach, preformed micelles were exposed to C_{60}/C_{70} through sonication in water. Crosslinking was then performed to lock the C_{60}/C_{70} that entered into the core. Alternatively, polymer and C_{60}/C_{70} were mixed together in tetrahydrofuran, and then water was added to allow the formation of micelles. Finally, the supramolecular structure was crosslinked. In the second approach, the polymer chains can interact with the fullerenes before formation of the secondary structure. To study the loading capacity arising from these different preparation methods, UV-Vis spectroscopy was used (ESI Fig. S3†). In water, the molar absorption coefficient (ε) of C_{60} is 49 000 at 340 nm, and 34 000 for C_{70} at 384 nm.[15] This allows a comparison to be made and calculation of the concentration of fullerenes in the crosslinked

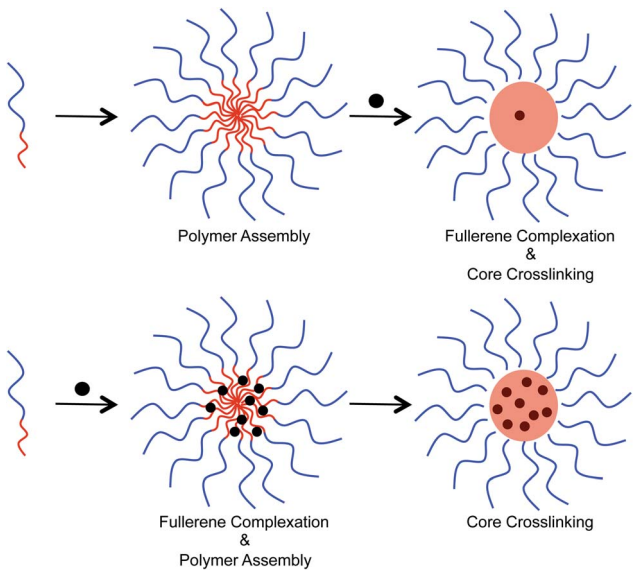

Fig. 4 Different approaches for the encapsulation of fullerenes into the host polymer micelle. The top shows exposure of pre-formed micelles to fullerenes, which leads to low fullerene loading capacity. The bottom shows an alternative approach in which the micelles are allowed to form in the presence of fullerenes leading to a higher fullerene loading capacity.

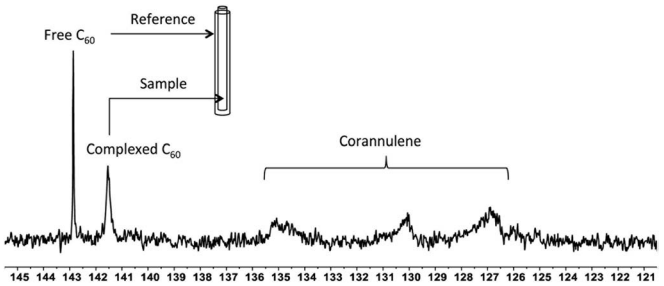

Fig. 5 ^{13}C NMR showing signals from the free C_{60} added as an external standard in the outer tube (reference) in deuterated tetrachloroethane and complexed C_{60} within the core of the crosslinked nanoparticle present in the inner tube (sample) also in deuterated tetrachloroethane. The internal tube diameter was 3 mm, while the external tube diameter was 5 mm.

nanoparticles to be performed. These data indicated that the first approach resulted in the incorporation of approximately 1.22 wt% fullerenes into the particle core. The second approach, however, was superior and furnished 8.12 and 8.01 wt% C_{60} and C_{70}, respectively, into the nanoparticles.

To investigate the supramolecular complexation between fullerenes and corannulene through interaction of their curved surfaces, ^{13}C-enriched fullerenes were utilized, and the crosslinked nanoparticles were studied with the help of ^{13}C NMR spectroscopy (Fig. 5). In the case of C_{60} nanoparticles, an upfield shift of 1.4 ppm ($\delta = 142.8$ free C_{60}; $\delta = 141.4$ complexed C_{60}), indicative of aromatic shielding effect and consistent with the previously reported supramolecular fullerene complexes,[33] was observed in the ^{13}C resonance of C_{60}. To rule out any unspecific interactions as the cause for this shift, an external standard tube (of larger diameter than that of the original NMR tube) containing a pure solution of C_{60} in deuterated tetrachloroethane was used. These samples showed signals from the uncomplexed fullerene (present as an external standard) and the signal from the C_{60} nanoparticles also in deuterated tetrachloroethane. These data confirmed that the shift of 1.4 ppm was due to specific complexation of C_{60} with corannulenes in the nanoparticle core. A broadening of the C_{60} signal was also observed, possibly as a result of the restricted rotational freedom of complexed C_{60} molecules in the nanoparticle core.

Unlike C_{60}, which possesses only one type of carbon atom, C_{70} possesses 5 different types of carbons. Furthermore, the commercially obtained ^{13}C-enriched C_{70} sample was found to be contaminated with C_{60}. Therefore, the ^{13}C NMR displayed a total of 6 signals from a mixture of fullerenes (ESI Fig. S4†). The same external standard technique was employed to confirm the signal shift. This study indicated that in the nanoparticles, the signals shifted by approximately 1, 1.2, 1.5, 1.1, and 1.1 ppm upon C_{70} complexation. The signals were also relatively broad. These results again indicated that the fullerenes were localized in the particle core. Interestingly, when the two fullerenes are part of the same nanoparticle core, the shift in the C_{60} signal is nearly half (0.7 ppm) that when there is no competition from C_{70}. This indicates that C_{70} is a preferred guest and binds more strongly to the multicorannulene host. In DLS, the

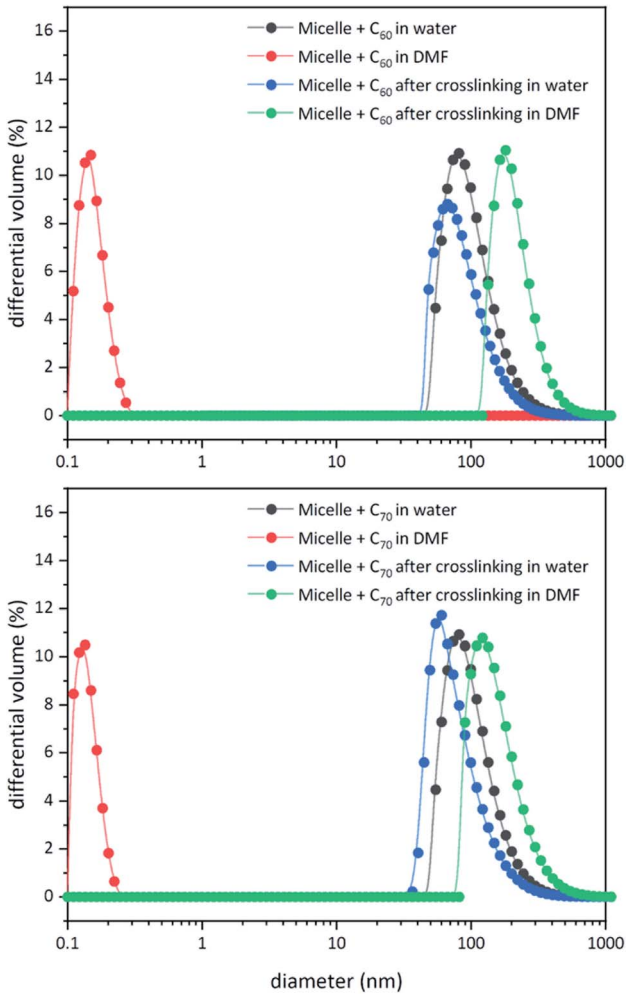

Fig. 6 DLS data for block copolymer micelles before and after core-crosslinking in water and DMF in the presence of C_{60} (top) and C_{70} (bottom).

nanostructure sizes increase when the core nests the fullerenes (Fig. 6). In transmission electron microscopy (TEM), these cores could be visualized without the need for staining the samples due to their high electron densities (Fig. 7 and ESI Fig. S5†).

Finally, corannulene was replaced with a simple phenyl group in polymer **1** (Scheme 3). This effort was directed at examining the antithesis that fullerene encapsulation in the micellar core required only a hydrophobic atmosphere and simple aromatic groups for stabilization. For this, the ring opening reaction was carried out using thiophenol to give polymer **2** (ESI Fig. S6†). Polymers **1** and **2** were obtained from the same PEG-*b*-PGMA scaffold. Hence, they contained identical number of repeating units in the polymer chains ($m \approx 113$, $n \approx 17$) necessary for comparison. Polymer **2** successfully formed micelles in water (ESI Fig. S7†). Importantly, however, it failed to show any fullerene uptake in its micellar core (ESI Fig. S8†).

The ^{13}C NMR and UV-Vis spectroscopies, therefore, suggest that the specific convex–concave interactions between fullerenes and corannulene are key to encapsulating a large amount of fullerenes in the nanoparticle core.

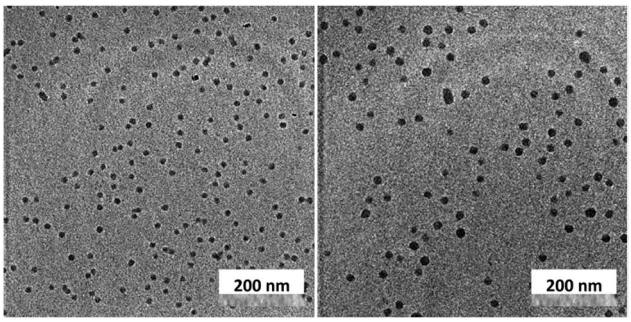

Fig. 7 Transmission electron microscopy images of the fullerene C_{60} (left) and C_{70}-loaded (right) nanoparticle cores.

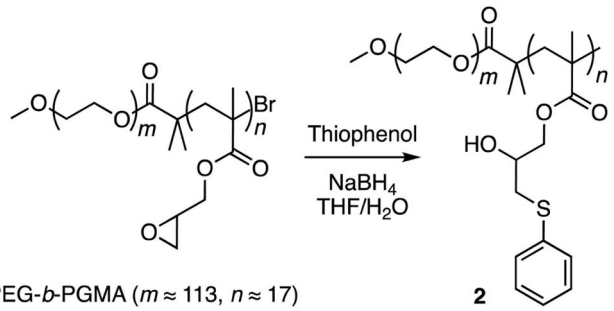

Scheme 3 Synthesis of copolymer **2**.

Structural integrity of the nanoparticles

Typically, aqueous dispersions of fullerene nanoparticles are prone to aggregation in the drying process, thereby losing their structural integrity. In the current molecular design, the particle shells are noncrosslinked and provide a molecularly defined layer of solvation (hydration) and protection to the crosslinked core against changes in concentration. The removal of the solvent and a redispersion therefore do not lead to any adverse effect on the integrity of the nanoparticles. This can be observed by drying the nanoparticulate matter and then redissolving it in water. The hydrodynamic volume before and after this process remains unchanged (ESI Fig. S9–S11†). This characteristic allows nanoparticles to be stored and transported in a powdered form. The aqueous solution can be prepared when required. Furthermore, once the solution is prepared, no changes are observed in the particle sizes even for months after their dissolution (ESI Fig. S12†).

Encouraged by these results, the thermal stability of the cargo was studied with the help of ^{13}C NMR spectroscopy (Fig. 8). The goal of these experiments was to heat the nanoparticles and determine whether uncomplexed fullerene could be detected in solution. If so, it would indicate that the guest-loaded core is unstable at higher temperatures and releases the guest molecules into the solution. In these experiments, an external standard was not employed to avoid overlap between the free fullerene signals. Initially, the C_{60}-containing nanoparticles were heated at 60 °C for 24 hours, and no signal belonging to the free fullerene could be observed in the

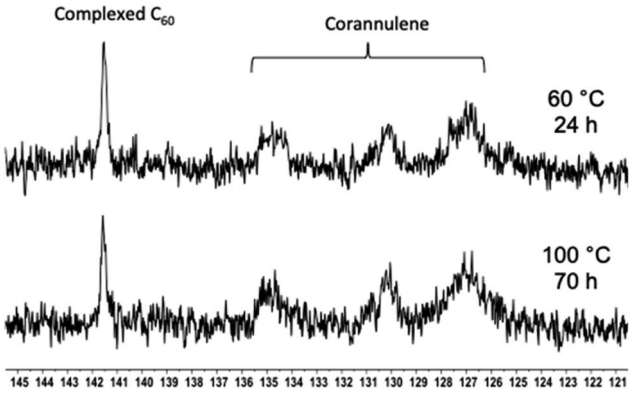

Fig. 8 ^{13}C NMR spectra showing the C_{60} signal in the polymer nanoparticle core after heating at 60 (top) and 100 °C (bottom) for 24 and 70 hours, respectively.

solution. Therefore, the temperature was increased to 100 °C, and the sample was heated for 70 hours. In this case also, the complexed fullerene signal remained intact.

Finally, nanoparticle stability was evaluated against acidic and basic conditions. For this, nanoparticles were dissolved in PBS (pH = 7.4) and citric acid/Na_2HPO_4 (pH = 2.5) buffers and monitored with the help of DLS. The nanoparticles did not display any change in their diameter under either conditions (ESI Fig. S13†).

The ability to switch from bulk materials to aqueous solution and withstand demanding thermal/pH conditions relates to the core–shell morphology of the nanostructures and is unprecedented in the fullerene-based water-soluble nanoparticle arena.

Radical scavenging activity

Having access to fullerene nanoparticles, their free radical scavenging activity was assessed with the help of a 2,2′-azinobis(3-ethylbenzothiazoline-6-sulfonic acid) (ABTS) assay.[34] In this assay, the interaction between an antioxidant and the pregenerated ABTS radical cation was examined with the help of UV-Vis spectroscopy (Fig. 9). Upon successful quenching of the radical cation, a decrease in the absorption intensity of the signals located at 645, 734, and 815 nm could be observed. The amount of antioxidant required to quench this intensity by 50% is defined as the inhibition concentration$_{50}$ (IC_{50}). This study produced interesting results. The micelles without C_{60} show moderate antioxidant capacity (Fig. 9a), most likely due to

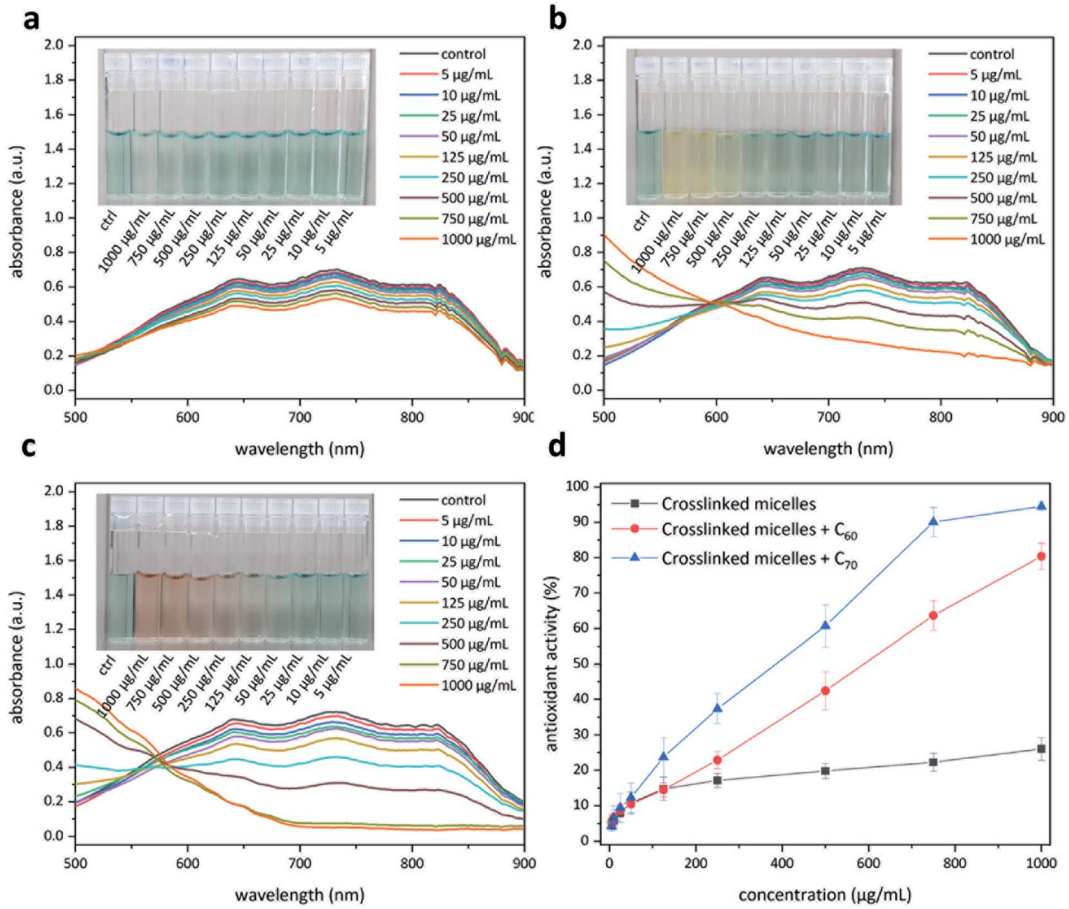

Fig. 9 Antioxidant activity of the polymer nanoparticles with and without fullerenes. Polymer nanoparticles without fullerenes (a). Polymer nanoparticles with fullerene C_{60} (b). Polymer nanoparticles with fullerene C_{70} (c). A comparison of the three systems to evaluate the amount needed to quench 50% of the free radicals in the system (d).

corannulenes in the micellar core ($IC_{50} \geq 1000$ μg mL^{-1}). The presence of C_{60} enhanced this capacity ($IC_{50} = 529$ μg mL^{-1}) (Fig. 9b). In the case of C_{70}, the visual color changes could already be appreciated beginning at 100 μg mL^{-1} (Fig. 9c). In this system, to reach IC_{50}, a relatively lower amount of 384 μg mL^{-1} was required. C_{70}-containing nanoparticles, therefore, are the most active system in this regard (Fig. 9d).

Protein adsorption

This aspect was studied with the help of bovine serum albumin (BSA) and the Bradford method to quantify the amount of the adsorbed protein onto the nanoparticles.[35] In this method, binding of the protein to a dye molecule changes its absorbance from red to blue region (ESI Fig. S14†). If no protein binds, then the solution remains brown. Thus, the amount of complex present in solution is a measure of the protein concentration and can be estimated by use of an absorbance reading. To achieve this, the particles were incubated with BSA for 3 hours to achieve equilibration. After this time, the particles were removed from the solution by centrifugation, and the supernatant was examined by means of UV-Vis spectroscopy (595 nm) to quantify the amount of the 'free' (unadsorbed) protein. In this way, the amount of adsorbed protein was calculated to be 3.5 and 3.8% for nanoparticles containing C_{60} and C_{70}, respectively.

Hemolysis

As a measure of biocompatibility, a hemolysis assay was performed to assess the lytic activity of nanoparticles using sheep red blood cells (RBCs). In this study, the released hemoglobin was detected by means of UV-Vis spectroscopy at a wavelength of 540 nm and compared to positive and negative controls. The negative control was PBS buffer, in which the RBCs do not disintegrate owing to the isotonic effect and a net zero movement of molecules across the membrane.[36] The positive control was deionized water, in which RBCs disintegrate fully due to a hypotonic effect and movement of pure water into the cells through osmosis, resulting in bursting of the cell walls. In the case of nanoparticles, however, no hemolysis was observed even at a concentration of 1000 μg mL^{-1} (ESI Fig. S15†). This suggests that nanoparticles have no toxic effects on mammalian cell walls, which bodes well for their future applicability as diagnostic probes.

Conclusions

In summary, core-crosslinked polymer nanoparticles can be prepared by combining a supramolecular complexation and covalent stabilization strategy. The particles contain a high loading (8%) of smaller (C_{60}) and larger (C_{70}) fullerenes and provide an opportunity to compare their properties. Radical scavenging leads to the conclusion that C_{70} particles possess higher antioxidant activity ($IC_{50} = 384$ μg mL^{-1}). The particles can be stored in a powdered form in bulk and can be redispersed when required. They are stable even when heated to 100 °C for 70 hours. They resist the accumulation of proteins (<4%) and are nonhemolytic even at high concentrations (1000 μg mL^{-1}). It is anticipated that replacing normal fullerenes from the present design with endohedral fullerenes containing a contrast agent, such as Gd(III), will lead to nontoxic imaging probes with long circulation times due to their nanometer sizes and a poly(ethylene glycol) shell. Furthermore, the preparation of water-soluble nanoparticles with higher fullerenes[37] (*e.g.*, C_{76} and C_{84}) and the study of their biorelevant properties appear to be an enticing research direction.

Experimental details

Micelle formation

First approach. Diblock copolymer **1** (3 mg) was first dissolved in THF (150 μL). After adding this suspension dropwise into deionized water (3 mL) under stirring, the micellar solution was dialyzed (dialysis tube: cutoff 1 kDa) against deionized (DI) water for 2 days to remove the THF. The final polymer concentration was about 1 mg mL^{-1}. Fullerene (1 eq. per corannulene unit) was added into the micellar solution (3 mg mL^{-1}) and sonicated for 30 minutes. The solution was then filtered through a 0.8 μm syringe filter (cellulose acetate).

Second approach. Diblock copolymer **1** (3 mg) and fullerene (1 eq. per corannulene unit) were first suspended in THF (150 μL) and stirred for 30 minutes. After adding this suspension dropwise into deionized (DI) water (3 mL) under stirring, the micelle solution was then filtered through a 0.8 μm syringe filter (cellulose acetate). The mixture was dialyzed (dialysis tube: cutoff 1 kDa) against deionized water for 2 days to remove the THF.

Crosslinking of micelles

To a solution of adipic acid (0.15 mg, 1 μmol (0.5 eq. per hydroxyl unit)), EDCI (0.5 mg, 0.2 μmol) and DMAP (0.3 mg, 0.2 μmol) in DI water (50 μL) were added dropwise into the micellar solution (1 mg mL^{-1}). The reaction mixture was stirred at room temperature overnight. After this time, the reaction mixture was dialyzed (dialysis tube: cutoff 1 kDa) against DI water for 1 day. The crosslinked micelles were lyophilized to dryness.

Conflicts of interest

There are no conflicts to declare.

Acknowledgements

Financial support from the Ministry of Education Singapore under the AcRF Tier 1 (2019-T1-002-066) (RG106/19) (2018-T1-001-176) (RG18/18); Agency for Science, Technology and Research (A*STAR)-AME IRG A1883c0006; and NTU (04INS000171C230) is gratefully acknowledged. National Research Foundation of Korea grant funded by the Korean Government (MSIP) (NRF-18R1D1A1B07048527) is also acknowledged.

Notes and references

1 A. Hirsch, *Angew. Chem., Int. Ed.*, 1993, **32**, 1138–1141.
2 F. Diederich and C. Thilgen, *Science*, 1996, **271**, 317–323.
3 A. Hirsch and M. Brettreich, *Fullerenes: chemistry and reactions*, Wiley-VCH, Weinheim, 2005.
4 T. Akasaka, F. Wudl and S. Nagase, *Chemistry of nanocarbons*, John Wiley & Sons, Chichester, 2010.
5 (*a*) H. Kawagishi and T. Finkel, *Nat. Med.*, 2014, **20**, 711–713; (*b*) V. A. Chistyakov, Y. O. Smirnova, E. V. Prazdnova and A. V. Soldatov, *BioMed Res. Int.*, 2013, **2013**, 821498.
6 (*a*) A. A. Popov, S. F. Yang and L. Dunsch, *Chem. Rev.*, 2013, **113**, 5989–6113; (*b*) K. B. Ghiassi, M. M. Olmstead and A. L. Balch, *Dalton Trans.*, 2014, **43**, 7346–7358.
7 (*a*) J. G. Penfield and R. F. Reilly, *Nat. Clin. Pract. Nephrol.*, 2007, **3**, 654–668; (*b*) V. Gulani, F. Calamante, F. G. Shellock, E. Kanal and S. B. Reeder, *Lancet Neurol.*, 2017, **16**, 564–570.
8 For review articles, see: (*a*) F. Giacalone and N. Martín, *Chem. Rev.*, 2006, **106**, 5136–5190; (*b*) E. Badamshina and M. Gafurova, *J. Mater. Chem.*, 2012, **22**, 9427–9438; (*c*) P. Wilson, P. C. Ke, T. P. Davis and K. Kempe, *Eur. Polym. J.*, 2017, **88**, 486–515; (*d*) A. Ikeda, *J. Inclusion Phenom. Macrocyclic Chem.*, 2013, **77**, 49–65; (*e*) X. Y. Zhang, H. L. Cong, B. Yu and Q. Chen, *Mini-Rev. Org. Chem.*, 2019, **16**, 92–99.
9 J. F. R. Van Guyse, V. R. de la Rosa, R. Lund, M. De Bruyne, R. De Rycke, S. K. Filippov and R. Hoogenboom, *ACS Macro Lett.*, 2019, **8**, 172–176.
10 J. F. R. Van Guyse, V. R. de la Rosa and R. Hoogenboom, *Chem.–Eur. J.*, 2018, **24**, 2758–2766.
11 K. Kempe, A. Vollrath, H. W. Schaefer, T. G. Poehlmann, C. Biskup, R. Hoogenboom, S. Hornig and U. S. Schubert, *Macromol. Rapid Commun.*, 2010, **31**, 1869–1873.
12 J. Tong, M. C. Zimmerman, S. M. Li, X. Yi, R. Luxenhofer, R. Jordan and A. V. Kabanov, *Biomaterials*, 2011, **32**, 3654–3665.
13 M. S. Misirkic, B. M. Todorovic-Markovic, L. M. Vucicevic, K. D. Janjetovica, V. R. Jokanovic, M. D. Dramicanin, Z. M. Markovic and V. S. Trajkovic, *Biomaterials*, 2009, **30**, 2319–2328.
14 T. Andersson, K. Nilsson, M. Sundahl, G. Westman and O. Wennerstrom, *J. Chem. Soc., Chem. Commun.*, 1992, 604–606.
15 Y. N. Yamakoshi, T. Yagami, K. Fukuhara, S. Sueyoshi and N. Miyata, *J. Chem. Soc., Chem. Commun.*, 1994, 517–518.
16 M. Akiyama, A. Ikeda, T. Shintani, Y. Doi, J. Kikuchi, T. Ogawa, K. Yogo, T. Takeya and N. Yamamoto, *Org. Biomol. Chem.*, 2008, **6**, 1015–1019.
17 D. Antoku, K. Sugikawa and A. Ikeda, *Chem.–Eur. J.*, 2019, **25**, 1854–1865.
18 (*a*) A. Muñoz, D. Sigwalt, B. M. Illescas, J. Luczowiak, L. Rodríguez-Pérez, I. Nierengarten, M. Holler, J.-S. Remy, K. Buffet, S. P. Vincent, J. Rojo, R. Delgado, J.-F. Nierengarten and N. Martín, *Nat. Chem.*, 2016, **8**, 50–57; (*b*) B. M. Illescas, J. Rojo, R. Delgado and N. Martín, *J. Am. Chem. Soc.*, 2017, **139**, 6018–6025; (*c*) J. Ramos-Soriano, J. J. Reina, B. M. Illescas, N. de la Cruz, L. Rodríguez-Pérez, F. Lasala, J. Rojo, R. Delgado and N. Martín, *J. Am. Chem. Soc.*, 2019, **141**, 15403–15412.
19 (*a*) A. Ikeda, Y. Doi, M. Hashizume, J. Kikuchi and T. Konishi, *J. Am. Chem. Soc.*, 2007, **129**, 4140–4141; (*b*) Y. Doi, A. Ikeda, M. Akiyama, M. Nagano, T. Shigematsu, T. Ogawa, T. Takeya and T. Nagasaki, *Chem.–Eur. J.*, 2008, **14**, 8892–8897.
20 (*a*) Y. T. Wu and J. S. Siegel, *Chem. Rev.*, 2006, **106**, 4843–4867; (*b*) V. M. Tsefrikas and L. T. Scott, *Chem. Rev.*, 2006, **106**, 4868–4884; (*c*) A. Sygula, *Eur. J. Org. Chem.*, 2011, 1611–1625; (*d*) A. M. Rice, E. A. Dolgopolova and N. B. Shustova, *Chem. Mater.*, 2017, **29**, 7054–7061; (*e*) E. Nestoros and M. C. Stuparu, *Chem. Commun.*, 2018, **54**, 6503–6519; (*f*) A. Haupt and D. Lentz, *Chem.–Eur. J.*, 2019, **25**, 3440–3454.
21 W. E. Barth and R. G. Lawton, *J. Am. Chem. Soc.*, 1966, **88**, 380–381.
22 (*a*) S. Mizyed, P. E. Georghiou, M. Bancu, B. Cuadra, A. K. Rai, P. Cheng and L. T. Scott, *J. Am. Chem. Soc.*, 2001, **123**, 12770–12774; (*b*) A. Sygula, F. R. Fronczek, R. Sygula, P. W. Rabideau and M. M. Olmstead, *J. Am. Chem. Soc.*, 2007, **129**, 3842–3843; (*c*) V. Garcia-Calvo, J. V. Cuevas, H. Barbero, S. Ferrero, C. M. Alvarez, J. A. Gonzalez, B. D. de Grenu, J. Garcia-Calvo and T. Torroba, *Org. Lett.*, 2019, **21**, 5803–5807; (*d*) M. C. Stuparu, *Angew. Chem., Int. Ed.*, 2013, **52**, 7786–7790.
23 For review articles on concave–convex aromatic interactions, see: (*a*) E. M. Perez and N. Martín, *Chem. Soc. Rev.*, 2008, **37**, 1512–1519; (*b*) D. Canevet, E. M. Perez and N. Martín, *Angew. Chem., Int. Ed.*, 2011, **50**, 9248–9259; (*c*) E. M. Perez and N. Martín, *Chem. Soc. Rev.*, 2015, **44**, 6425–6433; (*d*) S. Selmani and D. J. Schipper, *Chem.–Eur. J.*, 2019, **25**, 6673–6692.
24 R. Duncan, *Nat. Rev. Drug Discovery*, 2003, **2**, 347–360.
25 For covalent stabilization of polymer nanostructures through chemical crosslinking process, see: K. L. Wooley, *J. Polym. Sci., Part A: Polym. Chem.*, 2000, **38**, 1397–1407.
26 L. F. Zhang and A. Eisenberg, *Science*, 1995, **268**, 1728–1731.
27 K. L. Wooley, *Chem.–Eur. J.*, 1997, **3**, 1397–1399.
28 C. F. van Nostrum, *Soft Matter*, 2011, **7**, 3246–3259.
29 M. Talelli, M. Barz, C. J. F. Rijcken, F. Kiessling, W. E. Hennink and T. Lammers, *Nano Today*, 2015, **10**, 93–117.
30 R. K. O'Reilly, M. J. Joralemon, K. L. Wooley and C. J. Hawker, *Chem. Mater.*, 2005, **17**, 5976–5988.
31 R. K. O'Reilly, C. J. Hawker and K. L. Wooley, *Chem. Soc. Rev.*, 2006, **35**, 1068–1083.
32 X. P. Dong, X. L. Guo, G. Q. Liu, A. P. Fan, Z. Wang and Y. J. Zhao, *Chem. Commun.*, 2017, **53**, 3822–3825.
33 (*a*) H. Isla, M. Gallego, E. M. Perez, R. Viruela, E. Orti and N. Martín, *J. Am. Chem. Soc.*, 2010, **132**, 1772–1773; (*b*) J. L. Wietor, G. D. Pantos and J. K. M. Sanders, *Angew. Chem., Int. Ed.*, 2008, **47**, 2689–2692; (*c*) A. R. Stefankiewicz, E. Tamanini, G. D. Pantos and J. K. M. Sanders, *Angew. Chem., Int. Ed.*, 2011, **50**, 5724–5727.

34 I. R. Ilyasov, V. L. Beloborodov, I. A. Selivanova and R. P. Terekhov, *Int. J. Mol. Sci.*, 2020, **21**, 1131.
35 M. M. Bradford, *Anal. Biochem.*, 1976, **72**, 248–254.
36 L. K. Goodhead and F. M. MacMillan, *Adv. Physiol. Educ.*, 2017, **41**, 298–305.
37 F. Diederich and R. L. Whetten, *Acc. Chem. Res.*, 1992, **25**, 119–126.